ADVANCED ENERGY MATERIALS
www.advenergymat.de

Multilayered-Electrode-Based Triboelectric Nanogenerators with Managed Output Voltage and Multifold Enhanced Charge Transport

*Gang Cheng, Li Zheng, Zong-Hong Lin, Jin Yang, Zuliang Du, and Zhong Lin Wang**

The open-circuit voltage of a triboelectric nanogenerator (TENG) increases with the tribo-charge density and the separated distance between two tribo-surfaces, which can reach several thousand volts and is much higher than the working voltage required by most electrical devices and energy storage units. Therefore, improving the effective efficiency of TENGs requires reducing the output voltage and enhancing the transferred charges. Here, a multilayered-electrode-based TENG (ME-TENG) is developed in which the output voltage can be managed by controlling the charge flow in a process of multiple (*N*) steps, which results in *N* times lower voltage but *N* times higher total charge transport. The ME-TENG is demonstrated to work in various modes, including multichannel, single-channel, and double-tribo-surface structures. The effects of insulator layer thickness and total layer number on the output voltage are simulated by the finite element method. The output voltage can be modulated from 14 to 102 V by changing the insulator layer number between two adjacent working electrodes, based on which the 8-bit logic representations of the characters in the ACSII code table are demonstrated. The ME-TENG provides a novel method to manage the output power and has potential applications in self-powered sensors array and human–machine interfacing with logic communications.

1. Introduction

In recent years, developing high-efficiency and low-cost methods for harvesting mechanical energy has attracted much interest.[1–4] Differing from previous methods based on electromagnetic,[5,6] electrostatic,[7,8] and piezoelectric[9–15] effects, triboelectric nanogenerator (TENG)[16–28] has been demonstrated to exhibit high efficiency, low cost, easy fabrication, and broad range of applications. Physically, when two materials with different triboelectric series are contacted, the tribo-charges with opposite polarities are generated on the surfaces of the two materials,[29–31] and the potential difference is generated when the two materials are separated, which can be used to drive the charge flow. Some electrical devices, including light-emitting diodes[21–25] and photodetectors,[28] can be powered by the TENG. Also, the generated energy of a TENG can be stored in a battery or a capacitor. By increasing the tribo-charges density and the separated distance between two tribo-surfaces, the open-circuit voltage of the TENG can reach several thousand volts,[21] which is much higher than the working voltage required by most electrical devices and energy storage units (typically ranging from several volts to several tens volts). Therefore, in order to improve the effective efficiency of the TENG, some methods have been developed to reduce the output voltage and enhance the total transferred charges.[32,33] For a radial-arrayed rotary TENG, a potential transformer has been used to reduce the output voltage and enhance the output current.[32] However, the potential transformer has high working frequency and low-input load resistance, which is difficult to match the low-frequency and high-output load resistance properties of a TENG. In addition, a power-transformed-and-managed system has been developed to reduce the output voltage and enhance the transferred charges for a TENG, which is based on a complex external circuit to switch the connection of multiple capacitors.[33]

Here, a multilayered-electrodes-based TENG (ME-TENG) is proposed and experimentally demonstrated. The output voltage of the ME-TENG can be managed by controlling the charge flow in a process of multiple steps (*N* steps), which results in *N* times lowering in voltage but *N* times increased in total charge transport. Two working modes, multichannel mode and single-channel mode have been developed in this ME-TENG. Also, a double tribo-surfaces structure has been designed to double the collected charges. The output voltage can be simply modulated by changing the insulator layer number between two adjacent

Dr. G. Cheng, Dr. L. Zheng, Dr. Z.-H. Lin, Dr. J. Yang, Prof. Z. L. Wang
School of Material Science and Engineering
Georgia Institute of Technology
Atlanta, Georgia 30332-0245, USA
E-mail: zlwang@gatech.edu
Dr. G. Cheng, Prof. Z. L. Du
Key Lab for Special Functional Materials
Henan University
Kaifeng 475004, China
Prof. Z. L. Wang
Beijing Institute of Nanoenergy and Nanosystems
Chinese Academy of Sciences
Beijing 100083, China

DOI: 10.1002/aenm.201401452

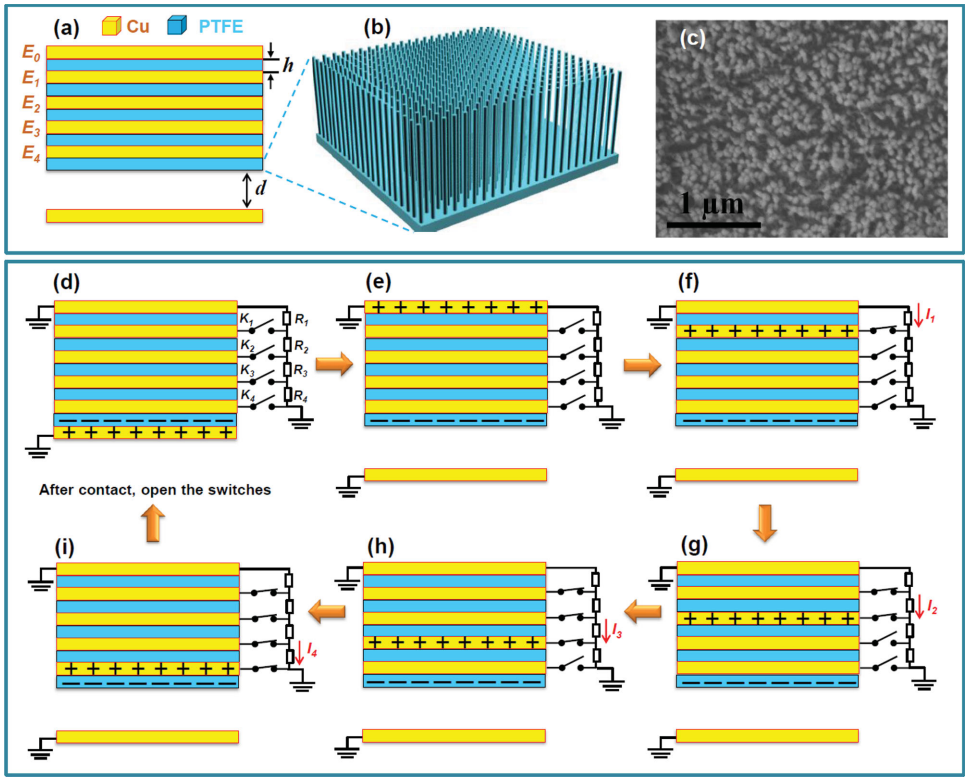

Figure 1. a) The structure diagram of a five-layer ME-TENG. b) The schematic diagram and c) SEM image of the nanorods fabricated by the AAO template method on the PTFE layer surface at bottom of the multilayer structure. d–i) The working mechanism of ME-TENG in multichannel mode.

working electrodes, based on which the ME-TENG is demonstrated to generate the 8-bit logic representations of the characters in the ACSII code table.

2. Results and Discussion

2.1. Multilayered Electrode Structure

The ME-TENG operates in a typical vertical contact-separation mode,[26] and its structure diagram is shown in **Figure 1**a. For the bottom plate, a 100-nm-thick Cu film was deposited on a square poly(methyl methacrylate) (PMMA) sheet by the e-beam evaporation method to serve as both the bottom electrode and one tribo-surface. For the top plate, a multilayered electrodes structure (MES) with alternating metal/insulator layers was attached to a PMMA sheet. The PMMA sheets on the top and bottom plates are not shown in Figure 1a for simplifying the diagram. The insulator layers in the MES were polytetrafluoroethylene (PTFE) films with a thickness (h) of 100 μm, and the metal-electrode layers of 100-nm-thick Cu film in the MES were deposited on the back side of each PTFE film. For a five-layer MES, as shown in Figure 1a, the five metal electrodes from top to bottom are defined as E_0, E_1, E_2, E_3, and E_4, respectively. The lowest PTFE layer (below E_4) was served as another tribo-surface, and high-density nanorods structure was fabricated on its surface by using porous anodic Al oxide (AAO) template method.[34] The structure diagram and the scanning electron microscopy (SEM) image of the PTFE nanorods are shown in **Figure 2**b,c, respectively. The mean length and diameter of the PTFE nanorods are 360 and 45 nm, respectively. The fabricated nanostructure on the tribo-surface can increase the contact area and improve the performance of a TENG.[21]

2.2. Multichannel Mode ME-TENG

At first, the ME-TENG is demonstrated to work at a multichannel mode, which is sketched in Figure 1d–i. For a five-layer MES, there are four electrical output channels, and each channel is formed between two adjacent Cu electrodes. R_1, R_2, R_3, and R_4 are the external-load resistances in the four channels, respectively, and K_1, K_2, K_3, and K_4 are corresponding switches to control the open/closed states of the four channels. The bottom electrode, E_0, and one terminal of K_4 are connected to the ground. As shown in Figure 1d, when the two tribo-surfaces are contacted together, positive and negative tribo-charges are generated on the bottom electrode and the PTFE layer, respectively, due to their different triboelectric polarities. With the moving up of the top plate, the two tribo-surfaces are separated, and a negative potential difference between E_0 and the bottom electrode is generated, which drives the positive charges in the bottom electrode to be transferred to E_0, as shown in Figure 1e. In an infinite approximation (the side length L of the device is infinite), the positive charges in E_0 and the negative charges in PTFE layer will generate a uniform electric field in the MES, and the potential differences between every two adjacent electrodes in the MES are equal and can be expressed as

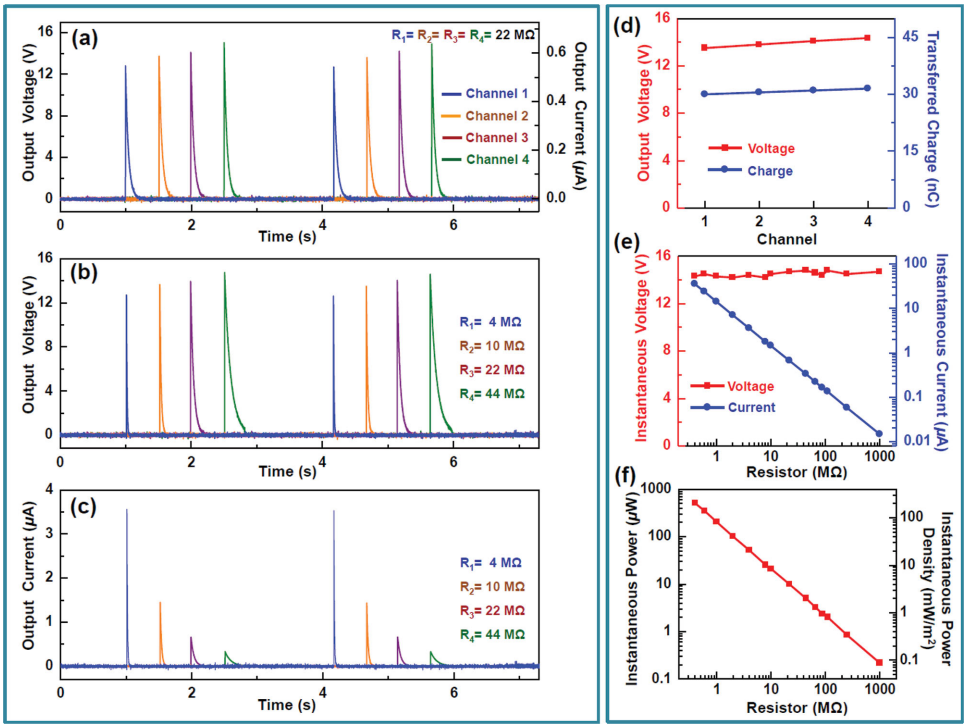

Figure 2. a) The output voltage and current curves of the four-channel ME-TENG with same load resistances, where the load resistance in each channel is 22 MΩ. b) The output voltage and c) current curves of the four-channel ME-TENG with various load resistances, and the load resistances in the four channels are 4, 10, 22, and 44 MΩ, respectively. d) The plots of voltage peaks and transferred charges in four channels. e) The dependence of instantaneous voltage and current peaks on the load resistances for channel 4. f) The dependence of instantaneous power and power density on the load resistances for channel 4.

$$V = \frac{\sigma}{\varepsilon} h \tag{1}$$

where σ is the tribo-charge density in the tribo-surface, h is the thickness of the PTFE layer, and ε is the permittivity of the PTFE layer. When the switch K_1 is closed, E_0 and E_1 are connected together, and the positive potential difference between them drives the positive charges to be transferred from E_0 to E_1, which generates a pulsed current peak in channel 1,[24,26] as shown in Figure 1f. Similarly, as the other three switches (K_2, K_3, and K_4) are closed in sequence, the positive charges are transferred to the next lower electrode step by step ($E_1 \rightarrow E_2 \rightarrow E_3 \rightarrow E_4$), and three pulsed current peaks are generated in channel 2, channel 3, and channel 4 sequentially (as shown in Figure 1g–i). When the top plate moves down and the two tribo-surfaces are contacted, the positive charges in E_4 are transferred to the bottom electrode, as shown in Figure 1a. After that, the four switches are opened, the top plate moves up again, and a new cycle starts.

The electrical output properties of the four channels were obtained by measuring the potential drop across the four load resistances by using four electrometers. As the load resistances of the four channels are equal ($R_1 = R_2 = R_3 = R_4 = 22$ MΩ), the voltage and current curves are shown in Figure 2a. Four peaks with similar peak heights and widths appear in sequence, which correspond to the pulsed output signals in the four channels, respectively. As the four load resistances are different ($R_1 = 4$ MΩ, $R_2 = 10$ MΩ, $R_3 = 22$ MΩ, and $R_4 = 44$ MΩ), the voltage peaks of the four channels have similar heights, while the peak widths increase with the increase of load resistance, as shown in Figure 2b. For the current peaks (Figure 2c), the peak in channel with lower resistance has higher peak height and narrower peak width. The voltage peak values of the four channels are plotted in Figure 2d, which slightly increase from 13.5 V at channel 1 to 14.4 V at channel 4. By integrating the current curve, the transferred charges in the four channels are obtained and plotted in Figure 2d, which slightly increase from 30.1 nC at channel 1 to 31.5 nC at channel 4. As mentioned above, the output voltage values of the four channels are equal for an infinite approximation. The slight variations of the voltage peaks and the transferred charges are caused by the finite size of a practical device, which will be discussed in detail by the finite element method (FEM) later.

The electric output signals in the four channels are generated instantaneously as the switches are closed, which belong to a pulse mode TENG.[26] For a pulse mode TENG, the instantaneous output voltage does not vary with the load resistance R, the peak width increases linear with R, and the instantaneous current and power are linear with $1/R$. The resistance-dependent properties of the four channels ME-TENG were also measured, which have similar properties. Taking channel 4 as an example (as shown in Figure 2e,f), the measured instantaneous voltage in a range from 0.4 MΩ to 1 GΩ keeps constant around 14.3 V, and the measured instantaneous current and power are both linear with $1/R$ and decrease from 35.8 μA and 0.51 mW at a resistance of 0.4 MΩ to 14.7 nA and 0.22 μW at a resistance of 1 GΩ,

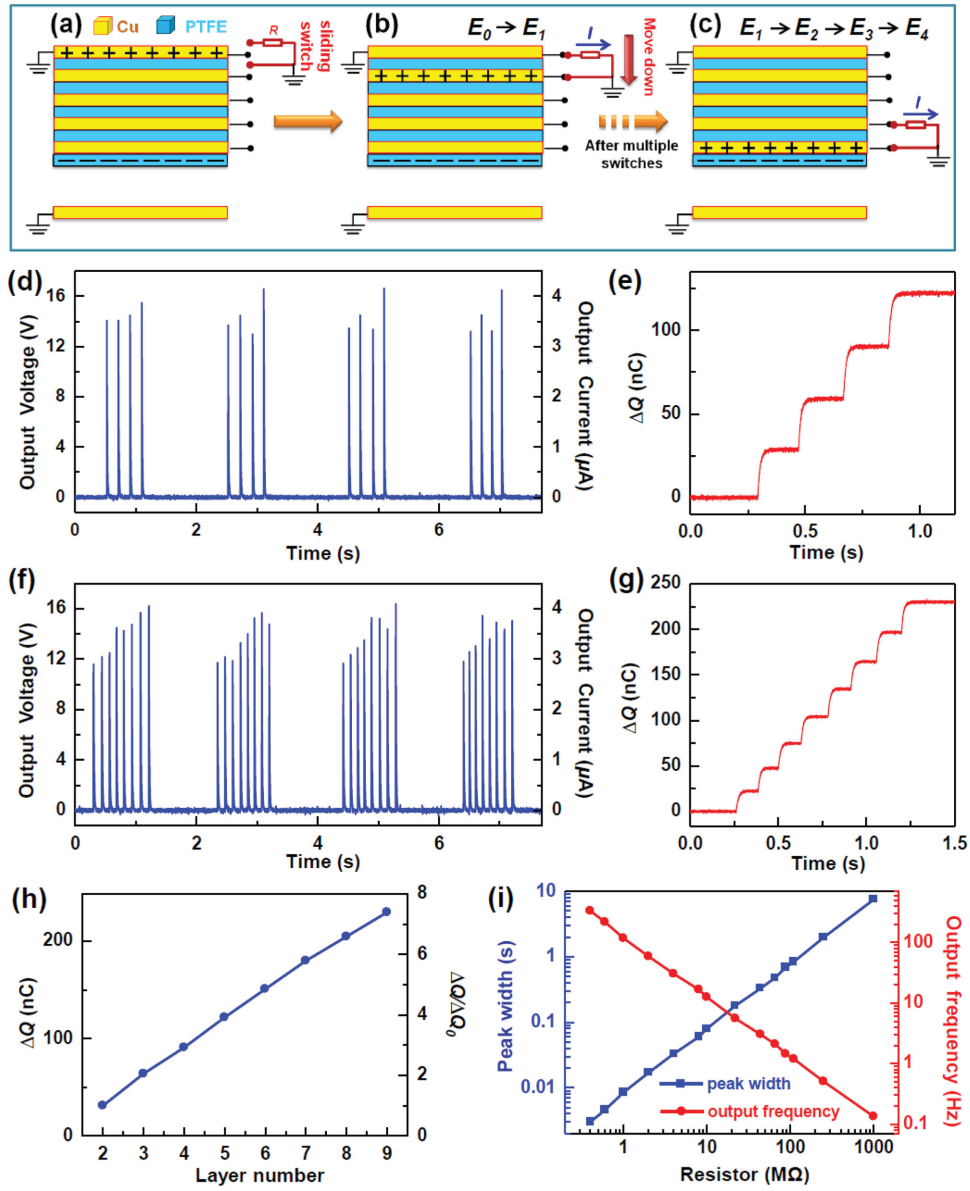

Figure 3. a–c) The working mechanism of the ME-TENG in single-channel mode, in which a sliding switch is used to collect all the transferred charges in a collecting electric channel. The output voltage and current curves with a load resistance of 4 MΩ for d) a five-layer and f) a nine-layer single-channel ME-TENG. The transferred charge curves of e) a five-layer and g) a nine-layer single-channel ME-TENG. h) The dependence of total-transferred charge in a cycle on the layer number in a multilayer structure. i) The dependences of output peak width and maximum output frequency of the ME-TENG on the load resistance.

respectively. When a TENG is used as a power source of a self-powered sensor, it is required that the TENG can match the resistance of the sensor, which means that the instantaneous current can vary with the variation of the sensor's equivalent resistance. For a traditional TENG, the instantaneous current keeps constant when the load resistance is lower than about 1 MΩ,[16–22] which limits its application in self-powered sensors. While, for a pulse TENG, the instantaneous current is nearly linear with $1/R$ in a range from 500 Ω to 1 GΩ,[26] which shows excellent resistance match performance. The multichannel mode ME-TENG can provide nearly equal voltage for different electrical channels, and all of the channels can match a large resistance range, which show its promising application as a multichannel power source in a self-powered sensors array consisting of lots of electronic and optoelectronic devices with a large resistance distribution range.

2.3. Single-Channel Mode ME-TENG

In case the ME-TENG is used to power a single device or store all the transferred charges in the MES into a single capacitor or battery, it is necessary to collect all of the generated current/charges into a single electric channel. Therefore, a single-channel mode of the ME-TENG is developed by using a sliding switch, and the working mechanism of a device with five-layer MES is sketched in **Figure 3**a–c. For the MES in the top plate,

each Cu electrode is connected to a stationary contact point. A collecting electric channel consists of a resistance R and two sliding contact points. The two sliding contact points move together and serve as a sliding switch. As shown in Figure 3a, when the two tribo-surfaces are separated, positive charges are transferred from bottom electrode to E_0, which is similar to the corresponding process in multichannel mode (Figure 1e). As the sliding switch begins to move from top to lower position, the top two electrodes, E_0 and E_1, are first connected by the sliding switch, the positive charges in E_0 are instantaneously transferred to E_1, and a pulsed current is generated in the collecting electric channel (as shown in Figure 3b). When the sliding switch continues to move downward, the adjacent two electrodes are connected together in sequence, and positive charges in the MES are transferred to the next lower electrode step by step ($E_1 \rightarrow E_2 \rightarrow E_3 \rightarrow E_4$), as shown in Figure 3c. During these processes, all the transferred charges are collected in one single channel, and multiple pulsed current peaks are generated in this channel. In the following, when the two tribo-surfaces are contacted, the positive charges are transferred from E_4 to the bottom electrode, which is similar to the corresponding process in multichannel mode (Figure 1d) and not shown here for simplification. It is worth noting here that for both multichannel and single-channel modes, the transferred charges in the separation and contact processes between the two tribo-surfaces (from bottom electrode to E_0, and from E_4 to bottom electrode) are not measured and collected. However, in these two processes, the device is in short-circuit condition without load resistance, and the output voltage is nearly equal to zero;[26] therefore, the output power and energy in these two processes are negligible.

The electric output properties of a five-layer ME-TENG in single-channel mode were measured. Figure 3d shows the output voltage and current curves, in which the load resistance in the collecting electric channel is 4 MΩ. Four pulsed output peaks are generated in a single cycle, and the voltage and current peaks are around 14.3 V and 3.6 μA, respectively. In the four pulsed peaks, the peaks height increases slightly in sequence, which is similar to that for the multichannel mode. As shown in Figure 3e, the measured charge curve consists of four steps, and each step corresponds to a charge transferring process between two adjacent electrodes. The height of each step is about 30.6 nC, and the total collected charge in a single cycle is about 122.4 nC. In order to further increase the number of the output peaks and enhance the total collected charge, a device with nine-layer MES is fabricated. As shown in the measured output curve with a load resistance of 4 MΩ (Figure 3f), eight pulsed output peaks are generated in a single cycle, in which the voltage peak gradually increases from about 11.8 to 15.6 V, and the current peak gradually increases from 3.0 to 3.9 μA. As shown in Figure 3g, the measured charge curve of the nine-layer ME-TENG consists of eight steps, the height of each step is about 28.8 nC, and the total collected charge in a single cycle is about 230.4 nC. The dependence of the total collected charge (ΔQ) on the layer number in the MES (N) ranging from 2 to 9 are plotted in Figure 3h. It is clear that ΔQ are nearly linear with N-1, and the ratio of $\Delta Q/\Delta Q_0$ increases to 7.4 as $N = 9$, where ΔQ_0 is the collected charges as the device works as a traditional contact-separation TENG. The results confirm that the single-channel ME-TENG can effectively enhance the collected charges. According to the working mechanism of the ME-TENG, only after the previous charge transfer process (from E_{n-1} to E_n) is completed, the next process (from E_n to E_{n+1}) is allowed to begin. Therefore, the allowed maximum output frequency is limited by the speed of the charge-transfer process, which is determined by the load resistance in the collecting electric channel. The values of peak width and the corresponding maximum output frequency at various load resistances ranging from 0.4 MΩ to 1 GΩ are shown in Figure 3i, respectively. It is indicated that the peak width increases linear with R from 3.1 ms at $R = 0.4$ MΩ to 7.5 s at $R = 1$ GΩ, and the corresponding maximum output frequency decreases from 322.6 to 0.13 Hz. The moving speed of the sliding switch should be properly set to avoid exceeding the allowed maximum output frequency.

2.4. Finite Element Simulation

According to Equation (1), the multiple peaks in a single cycle should have equal height in infinite approximation (the side length L of the device is infinite). While, in the measured curves for multichannel and single-channel modes, it is found that the output voltage peaks increase slightly when the charges in the MES are transferred from top layer to lower layers, which deviates from the infinite approximation. In order to investigate its origin, the 3D FEM was used to study the effects of device size on the output properties of the ME-TENG. At first, for a ME-TENG with a constant L (the side length of the square device) of 50 mm, the potential differences between the bottom two electrodes in the MES were calculated as the PTFE layer thickness (h) increases from 0 to 5 mm, and the calculated relation between V and h/L is plotted in **Figure 4**a. It is indicated that V increases nearly linearly with h/L as h/L is less than 0.02, while the slope of the curve gradually decreases as h/L is higher than 0.02. As shown in the inset of Figure 4b, by setting $L = 50$ mm and $h = 0.5$ mm, the potential differences between the top two electrodes in the MES were calculated as H increases from 0 to 10 mm, where H is the vertical distance from the lower electrode to the charged PTFE film and is equal to $(N - 2)h$ by neglecting the thickness of Cu electrode, and N is the number of PTFE layers in the MES. As shown in Figure 4b, the calculated voltage is reduced from 786 to 608 V as H/L increases from 0 to 0.2. The corresponding voltage-reduced ratio was calculated and shown in Figure 4c, which increases from 0% to 22.7% as H/L increases from 0 to 0.2. The calculated results in Figure 4b,c indicate that the output voltage of two higher electrodes should be lower than that of two lower electrodes, which can well explain the voltage variation of the multiple peaks in our experiment.

The FEM simulation results indicate that the output voltage of the ME-TENG can be effectively controlled by modulating the PTFE layer thickness h in the MES. While in the practical application, it is inconvenient to change h value for a fabricated device. Here, it is demonstrated that the output voltage can be simply modulated by changing the insulator layer number between two adjacent working electrodes. As shown in Figure 4d, two PTFE layers exist between two adjacent working

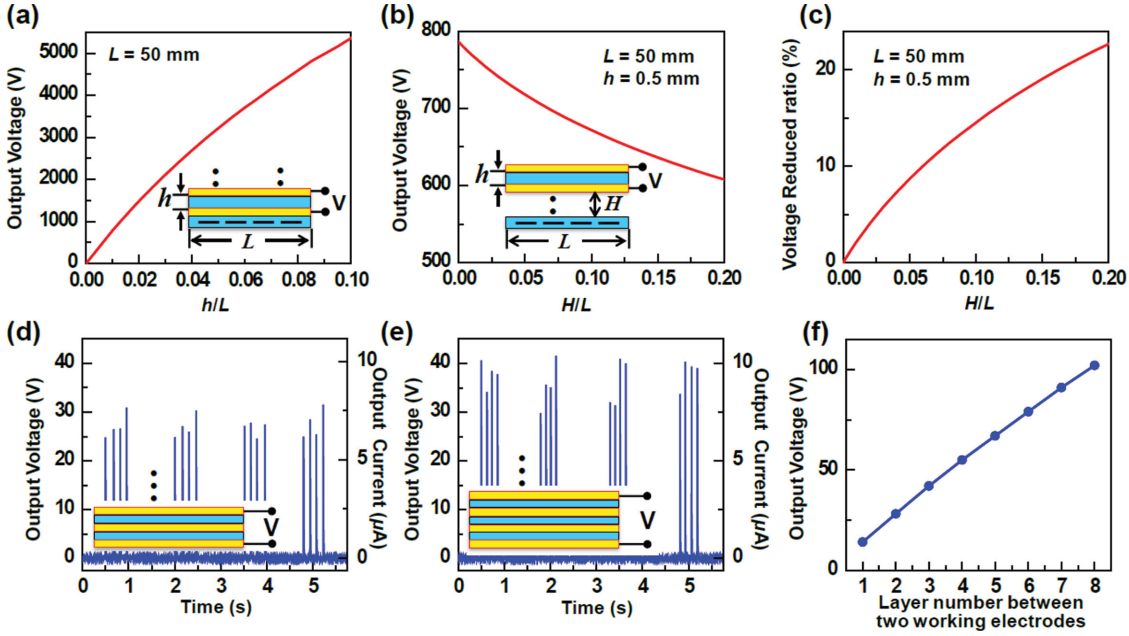

Figure 4. a) The dependence of the calculated output voltage on h/L ratio, where L is set as 50 mm. The dependences of b) the calculated output voltage and c) its reduced ratio on H/L ratio, where L and h are set as 50 and 0.5 mm, respectively. d,e) The measured output curves with a load resistance of 4 MΩ when two and three PTFE layers exist between two adjacent working electrodes, respectively, and the corresponding diagrams are shown in their insets. f) The dependence of output voltage on PTFE layer number between two adjacent working electrodes.

electrodes (E_n and E_{n+2}), and the output voltage peaks are around 28.2 V. As shown in Figure 4e, three PTFE layers exist between two adjacent working electrodes (E_n and E_{n+3}), and the output voltage peaks are around 42.1 V. As shown in Figure 4f, the measured output voltage nearly increases linearly from 14.2 to 102.3 V, as the PTFE layer number between two adjacent working electrodes increases from 1 to 8.

2.5. Logic Representation by using the ME-TENG

Since the output voltage can be modulated by the PTFE layer number between two adjacent working electrodes (defined as M), the ME-TENG can be used to represent logic value. When M is set as 1 and 2, lower and higher voltage values should be obtained, which can be coded into logic "0" and "1," respectively. By designing the sequence of M values in the MES, the generated voltage peaks can be coded into a sequence of binary logic values, which represents a multibit logic value. Here, the ME-TENG is demonstrated to generate the 8-bit logic representations of the characters in the ACSII code table, and the examples for four characters, "T," "E," "N," and "G" are shown in **Figure 5**a–d, respectively. For character "T," the diagram of the electrode configuration in the MES is shown in the left part of Figure 5a, where the following nine electrodes, E_0, E_1, E_3, E_4, E_6, E_7, E_9, E_{10}, and E_{11}, are used as the working electrodes, and the corresponding M sequence in the MES is "12121211" as the charges are transferred from top electrode to lower electrodes. The measured voltage curve at this electrode configuration with a load resistance of 4 MΩ is shown in the right part of Figure 5a, in which eight voltage peaks with different heights are generated in sequence. Here, it is defined that the peaks lower and higher than 18 V is coded into logic "0" and "1," respectively. According to the heights of the eight peaks in Figure 5, this voltage curve can be coded into a sequence of binary values "01010100," which corresponds the logic representation of character "T" in the ACSII code table. By changing the electrode configuration structure, the eight peaks can also be coded into the logic representations of characters "E," "N," and "G," which are demonstrated in Figure 5b–d, respectively. For generating an n-bit logic representation, a layer number of $2n + 1$ in the MES is required. These results show the potential application of the ME-TENG in human-machine interfacing with logic communications.

2.6. ME-TENG with Double Tribo-Surfaces Structure

In the ME-TENG described above, the multiple steps charge transport in the MES exists only in the separation half-cycle, but not in the contact half-cycle, as shown in Figure 1d–i. In order to enhance the collected charges in a total cycle, a double tribo-surfaces structure has been designed. As shown in **Figure 6**a, a 10-layer MES can move up and down, and alternately gets contacted with top and bottom PTFE tribo-surfaces, which results in negative tribo-charges in the two PTFE tribo-surfaces and positive tribo-charges in top and bottom electrode layers in the MES. The working mechanism of the double tribo-surfaces structure is sketched in Figure 6b–e. When the MES gets contacted with the bottom PTFE tribo-surface, the lower electrode has more negative potential, and the positive charges are transferred from top layer to lower layers as the sliding switch moves downward. Oppositely, the positive charges are transferred from bottom layer to higher layers as

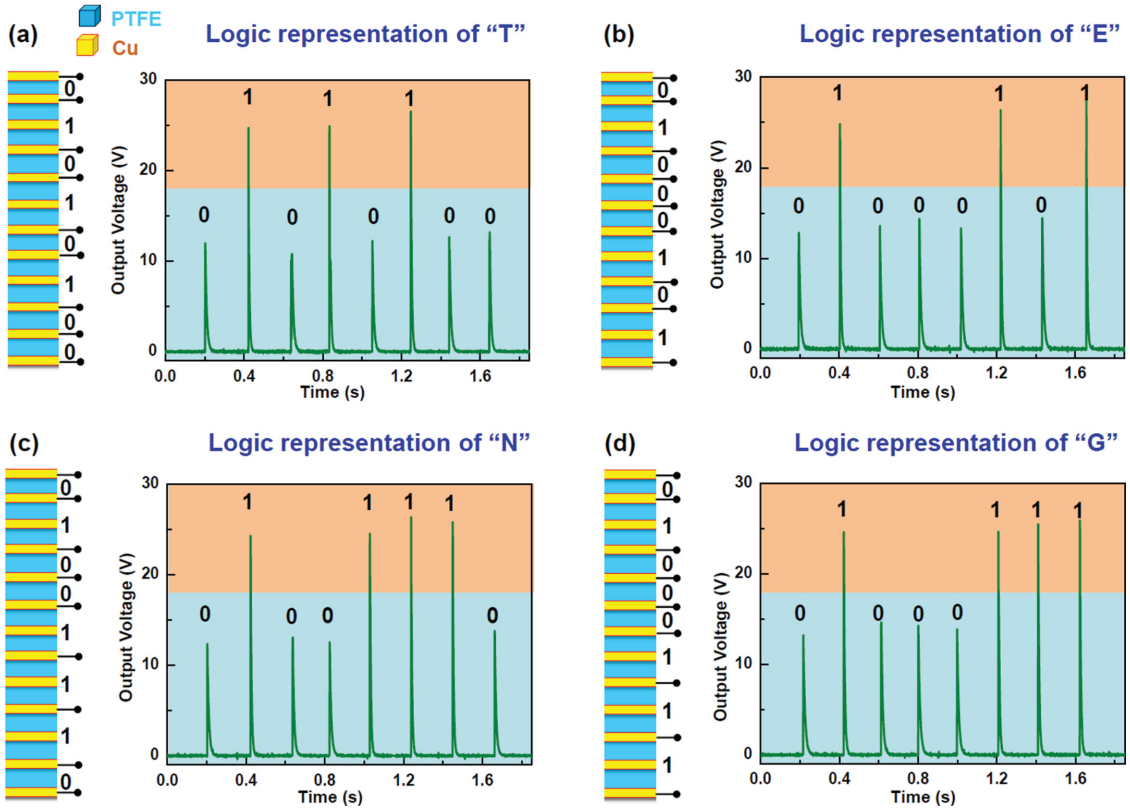

Figure 5. The electrodes configuration diagram and the output voltage curves for generating 8-bit logic representations of four characters, "T" a), "E" b), "N" c), and "G" d), in the ACSII code table. The output peaks lower and higher than 18 V are coded to logic "0" and "1," respectively.

the MES gets contacted with the top PTFE tribo-surface and the sliding switch moves upward. As a result, the charge-transport processes with multiple steps are generated in both the downward half-cycle and the upward half-cycle, which enhances the total collected charges in a whole cycle. It is noted that the distance between the two PTFE tribo-surfaces is 20 cm in our experiment, and the electrostatic effect of one PTFE tribo-surface is nearly negligible when the MES gets contacted with another PTFE tribo-surface. As shown in the output curve with a load resistance of 4 MΩ (Figure 6f), nine positive peaks followed by nine negative peaks are generated in a single cycle, which in good accordance with the charge-transfer processes described above. As shown in Figure 6g, the output peaks in the same direction can be obtained by using a full-wave rectifying bridge.

In order to compare the charging capacity, a 10-layer ME-TENG in different working modes (single-channel, multi-channel, and double tribo-surface modes) and the traditional TENG without the MES are used to charge a capacitor of 3.3 μF, in which the full-wave rectifying bridge is used. For multichannel mode ME-TENG, the capacitor is connected in one channel of the ME-TENG. As shown in Figure 6h, the time when the capacitor is charged to 6 V by using the double tribo-surface mode, single-channel mode, multichannel mode, and the traditional mode are 67, 127, 981, and 503 s, respectively. The lowest charging capacity of the multichannel mode is attributed to the fact that the charge transfers in the other eight electrical channels cannot be used to charge the capacitor. The highest charging capacity of the double tribo-surfaces mode is attributed to the multisteps charge transfers in both contact and separation half cycles.

3. Conclusion

An ME-TENG has been developed, in which the output voltage can be managed by controlling the charge flow in a process of multiple steps (*N* steps), which results in *N* times lowering in voltage but *N* times increased in total charge transport. In a multichannel mode, the ME-TENG can provide power sources with closely matched voltage for multiple electronic devices, which has potential applications in self-powered sensors array consisting of multiple sensors. In a single-channel mode, all the transferred charges in the MES can be collected into a single electrical output channel by using a sliding switch. The effects of insulator layer thickness and total layer number on the output voltage have been simulated by the FEM. The output voltage can be simply modulated from 14 to 102 V by changing the insulator layer number between two adjacent working electrodes, based on which it is demonstrated to generate the 8-bit logic representations of the characters in the ACSII code table. Also, a double tribo-surfaces structure has been developed, in which multiple steps charge transport can be generated in both the upward and the downward half-cycle. The proposed ME-TENG not only provides a novel method to manage the output voltage of a TENG but also has potential applications

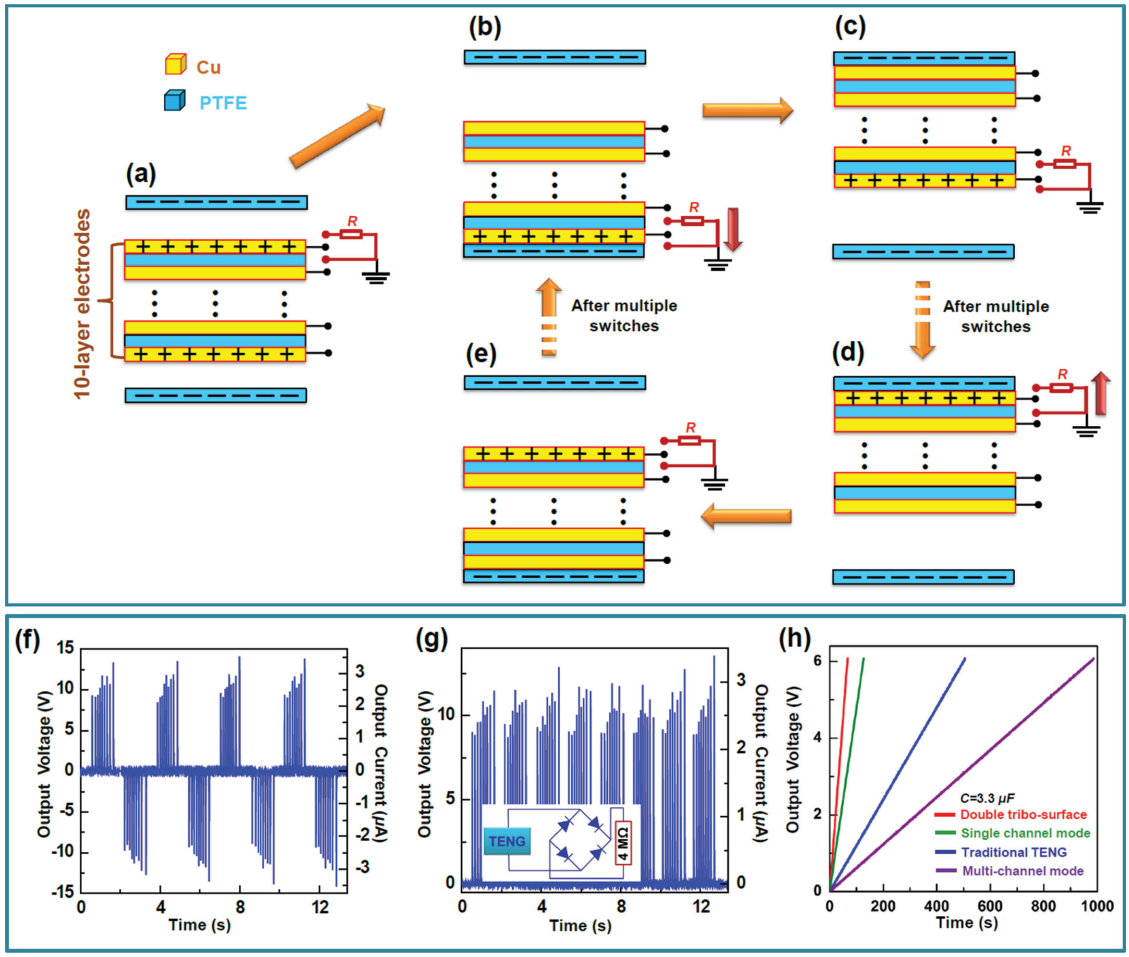

Figure 6. a–e) The working mechanism of the single-channel ME-TENG with double tribo-surfaces structure. f) The output voltage and current curves of a 10-layer structure at a load resistance of 4 MΩ. g) The diagram and the output curves in same direction after using a full-wave rectifying bridge. h) The voltage curves of a 3.3 μF capacitor charged by a 10-layer ME-TENG with various modes (single-channel, multichannel, and double tribo-surfaces structure modes) and by a traditional TENG, respectively, and a full-wave rectifying bridge was used in these cases.

in self-powered sensors array and human-machine interfacing with logic communications.

4. Experimental Section

Fabrication of the ME-TENG: A PMMA sheet (thickness of 0.3 cm) was processed by laser cutting (PLS6.75, Universal Laser Systems) to serve as the substrate of the plates, and the Cu films of thickness of 100 nm on bottom PMMA plate were deposited by the e-beam evaporation method. The commercial PTFE films of thickness of 100 μm were used to construct the multilayer structure, with acrylic adhesive on one side and 100-nm-thickness Cu film on the other side, which was deposited by the b-beam evaporation method. The PTFE layer with nanorods structure on the bottom of the multilayer structure was fabricated by porous AAO template methods: the PTFE solution was poured into the AAO template and a conventional vacuum process was applied to remove the air remaining in the nanoholes; after the curing at ambient temperature for 1 d, the solvent was evaporated; finally, the PTFE thin film was peeled off from the AAO template and was attached on the bottom of the multilayer structure by using a double-sided tape. The Cu sheets with width of 4 mm were attached on a PMMA sheet to serve as the electrical contact points of the electrodes in multilayer structure, the distance between two Cu sheets was 5 mm, and each contact point was connected to one electrode in the multilayer structure by using Cu wires.

Electric Measurement of the ME-TENG: In the electric output measurement, one plate was bonded onto a shaker for the vertical contact-separation motion, and the other plate was bonded onto a stationary stage. For multichannel mode, four commercial switches were controlled by the manual method. For single-channel mode, a homemade sliding switch (see photos in the Supporting Information) was controlled by a linear motor. The output voltage and transferred charges were measured by an electrometer (6514 system electrometer, Keithley). The voltages curves of the four channels for multichannel mode were simultaneously measured by using four electrometers.

Supporting Information

Supporting Information is available from the Wiley Online Library or from the author.

Acknowledgements

G.C. and L.Z. contributed equally to this paper. This work was supported by the Hightower Chair foundation, and the "thousands talents"

program for pioneer researcher and his innovation team, China, Beijing City Committee of science and technology (Z131100006013004, Z131100006013005). Patents have been filed based on the research presented here.

Received: August 20, 2014
Revised: October 19, 2014
Published online:

[1] Z. L. Wang, G. Zhu, Y. Yang, S. H. Wang, C. F. Pan, *Mater. Today* **2012**, *15*, 532.
[2] Z. L. Wang, W. Z. Wu, *Angew. Chem Int. Ed.* **2012**, *51*, 11700.
[3] S. P. Beeby, M. J. Tudor, N. M. White, *Meas. Sci. Technol.* **2006**, *17*, R175.
[4] P. D. Mitcheson, E. M. Yeatman, G. K. Rao, A. S. Holmes, T. C. Green, *Proc. IEEE* **2008**, *96*, 1457.
[5] C. B. Williams, C. Shearwood, M. A. Harradine, P. H. Mellor, T. S. Birch, R. B. Yates, *Proc. IEEE Circ. Dev. Syst.* **2001**, *148*, 337.
[6] S. P. Beeby, R. N. Torah, M. J. Tudor, P. Glynne-Jones, T. O'Donnell, C. R. Saha, S. Roy, *J. Micromech. Microeng.* **2007**, *17*, 1257.
[7] P. D. Mitcheson, P. Miao, B. H. Stark, E. M. Yeatman, A. S. Holmes, T. C. Green, *Sens. Actuators A* **2004**, *115*, 523.
[8] Y. Naruse, N. Matsubara, K. Mabuchi, M. Izumi, S. Suzuki, *J. Micromech. Microeng.* **2009**, *19*, 094002.
[9] Z. L. Wang, J. H. Song, *Science* **2006**, *312*, 242.
[10] Y. Qin, X. D. Wang, Z. L. Wang, *Nature* **2008**, *451*, 809.
[11] C. Xu, C. F. Pan, Y. Liu, Z. L. Wang, *Nano Energy* **2012**, *1*, 259.
[12] X. Chen, S. Y. Xu, N. Yao, Y. Shi, *Nano Lett.* **2010**, *10*, 2133.
[13] Y. F. Hu, L. Lin, Y. Zhang, Z. L. Wang, *Adv. Mater.* **2012**, *24*, 110.
[14] A. F. Yu, P. Jiang, Z. L. Wang, *Nano Energy* **2012**, *1*, 418.
[15] K. I. Park, M. Lee, Y. Liu, S. Moon, G. T. Hwang, G. Zhu, J. E. Kim, S. O. Kim, D. K. Kim, Z. L. Wang, K. J. Lee, *Adv. Mater.* **2012**, *24*, 2999.
[16] F. R. Fan, Z. Q. Tian, Z. L. Wang, *Nano Energy* **2012**, *1*, 328.
[17] F. R. Fan, L. Lin, G. Zhu, W. Z. Wu, R. Zhang, Z. L. Wang, *Nano Lett.* **2012**, *12*, 3109.
[18] H. L. Zhang, Y. Yang, T.-C. Hou, Y. J. Su, C. G. Hu, Z. L. Wang, *Nano Energy* **2013**, *2*, 1019.
[19] S. H. Wang, L. Lin, Z. L. Wang, *Nano Lett.* **2012**, *12*, 6339.
[20] X. S. Zhang, M. D. Han, R. X. Wang, F. Y. Zhu, Z. H. Li, W. Wang, H. X. Zhang, *Nano Lett.* **2013**, *13*, 1168.
[21] G. Zhu, Z.-H. Lin, Q. S. Jing, P. Bai, C. F. Pan, Y. Yang, Y. S. Zhou, Z. L. Wang, *Nano Lett.* **2013**, *13*, 847.
[22] P. Bai, G. Zhu, Y. Liu, J. Chen, Q. S. Jing, W. Q. Yang, J. S. Ma, G. Zhang, Z. L. Wang, *ACS Nano* **2013**, *7*, 6361.
[23] G. Zhu, P. Bai, J. Chen, Z. L. Wang, *Nano Energy* **2013**, *2*, 688.
[24] G. Cheng, Z.-H. Lin, Z. L. Du, Z. L. Wang, *Adv. Funct. Mater.* **2014**, *24*, 2892.
[25] L. Lin, S. H. Wang, Y. N. Xie, Q. S. Jing, S. M. Niu, Y. F. Hu, Z. L. Wang, *Nano Lett.* **2013**, *13*, 2916.
[26] G. Cheng, Z.-H. Lin, L. Lin, Z. L. Du, Z. L. Wang, *ACS Nano* **2013**, *7*, 7383.
[27] Y. Yang, H. L. Zhang, J. Chen, Q. S. Jing, Y. S. Zhou, X. N. Wen, Z. L. Wang, *ACS Nano* **2013**, *7*, 7342.
[28] Z.-H. Lin, G. Cheng, Y. Yang, Y. S. Zhou, S. M. Lee, Z. L. Wang, *Adv. Funct. Mater.* **2014**, *24*, 2810.
[29] G. S. P. Castle, *J. Electrostat.* **1997**, *40–41*, 13.
[30] L. S. McCarty, G. M. Whitesides, *Angew. Chem Int. Ed.* **2008**, *47*, 2188.
[31] J. A. Wiles, B. A. Grzybowski, A. Winkleman, G. M. Whitesides, *Anal. Chem.* **2003**, *75*, 4859.
[32] G. Zhu, J. Chen, T. J. Zhang, Q. S. Jing, Z. L. Wang, *Nat. Commun.* **2014**, *5*, 3426.
[33] W. Tang, T. Zhou, C. Zhang, F. R. Fan, C. B. Han, Z. L. Wang, *Nanotechnology* **2014**, *25*, 225402.
[34] G. Cheng, Z.-H. Lin, Z. L. Du, Z. L. Wang, *ACS Nano* **2014**, *8*, 1932.

